IJMMM International Journal of Minerals, Metallurgy and Materials 矿物冶金与材料学报（英文版）

Efficient AlN decomposition and Al species transformation in secondary aluminum dross through co-sintering with waste sodium acetate

Xiang Li, Nengwu Zhu, Yunhao Xi, Fei Li, and Pengfei Zhang

Cite this article as:
Xiang Li, Nengwu Zhu, Yunhao Xi, Fei Li, and Pengfei Zhang, Efficient AlN decomposition and Al species transformation in secondary aluminum dross through co-sintering with waste sodium acetate, *Int. J. Miner. Metall. Mater.*, 32(2025), No. 5, pp. 1079-1090. https://doi.org/10.1007/s12613-024-2990-9

View the article online at SpringerLink or IJMMM Webpage.

Articles you may be interested in

Bowei Zhang, Hezu Wang, Yan Su, Wenguang Yang, Xuelong Hao, Zequn Zhang, Fengqin Wang, Wei Xue, and Junsheng Wu, Secondary phase precipitate-induced localized corrosion of pure aluminum anode for aluminum–air battery, *Int. J. Miner. Metall. Mater.*, 30(2023), No. 5, pp. 977-987. https://doi.org/10.1007/s12613-022-2533-1

Guotao Zhou, Yilin Wang, Tiangui Qi, Qiusheng Zhou, Guihua Liu, Zhihong Peng, and Xiaobin Li, Comparison of the effects of Ti- and Si-containing minerals on goethite transformation in the Bayer digestion of goethitic bauxite, *Int. J. Miner. Metall. Mater.*, 30(2023), No. 9, pp. 1705-1715. https://doi.org/10.1007/s12613-023-2628-3

Hongyu Tian, Deqing Zhu, Jian Pan, Congcong Yang, Weiqun Huang, and Mansheng Chu, Effect mechanism of aluminum occurrence and content on the induration characteristics of iron ore pellets, *Int. J. Miner. Metall. Mater.*, 30(2023), No. 12, pp. 2334-2346. https://doi.org/10.1007/s12613-023-2725-3

Xuefeng Zhang and Shuqiang Jiao, Modified Al negative electrode for stable high-capacity Al–Te batteries, *Int. J. Miner. Metall. Mater.*, 29(2022), No. 4, pp. 896-904. https://doi.org/10.1007/s12613-022-2410-y

Long Wang, Liang Chen, Weizao Liu, Guoquan Zhang, Shengwei Tang, Hairong Yue, Bin Liang, and Dongmei Luo, Recovery of titanium, aluminum, magnesium and separating silicon from titanium-bearing blast furnace slag by sulfuric acid curing–leaching, *Int. J. Miner. Metall. Mater.*, 29(2022), No. 9, pp. 1705-1714. https://doi.org/10.1007/s12613-021-2293-3

Xiaoyu Zhang, Chunquan Li, Shuilin Zheng, Yonghao Di, and Zhiming Sun, A review of the synthesis and application of zeolites from coal-based solid wastes, *Int. J. Miner. Metall. Mater.*, 29(2022), No. 1, pp. 1-21. https://doi.org/10.1007/s12613-021-2256-8

IJMMM WeChat

QQ author group

INTERNATIONAL JOURNAL OF
Minerals, Metallurgy and Materials

Volume 32, Number 5, May 2025
Page 1079

Research Article https://doi.org/10.1007/s12613-024-2990-9

Efficient AlN decomposition and Al species transformation in secondary aluminum dross through co-sintering with waste sodium acetate

Xiang Li[1)], *Nengwu Zhu*[1,2,3,4),✉], *Yunhao Xi*[1)], *Fei Li*[1)], *and Pengfei Zhang*[1)]

1) School of Environment and Energy, South China University of Technology, Guangzhou 510006, China
2) The Key Laboratory of Pollution Control and Ecosystem Restoration in Industry Clusters Ministry of Education, Guangzhou 510006, China
3) Guangdong Environmental Protection Key Laboratory of Solid Waste Treatment and Recycling, Guangzhou 510006, China
4) Guangdong Provincial Key Laboratory of Solid Wastes Pollution Control and Recycling, Guangzhou 510006, China
(Received: 29 May 2024; revised: 31 July 2024; accepted: 21 August 2024)

Abstract: Secondary aluminum dross (SAD) is a rich source of recyclable aluminum but poses considerable risk due to its high AlN content. Therefore, thoroughly removing AlN is essential, but intricate aluminum components and expensive additives pose challenges to the process. In this study, waste sodium acetate is proposed as an environmentally friendly additive for completely removing AlN and enhancing the extraction of aluminum from SAD. Through the exothermic decomposition of NaAc, reactions can occur at 850°C. AlN removal efficiency reached 93.19% after sintering, whereas Al leaching efficiency in the subsequent leaching process reached 90.49%, which were 37.86% and 375.26% higher than the removal efficiency of the control, respectively. These favorable results were attributed to the comprehensive transformation of aluminum species. The formation of soluble phase $Na_{1.95}Al_{1.95}Si_{0.05}O_4$ occurred during the destruction of the Al_2O_3 layer surrounding AlN and the transformation of other aluminum components. AlN decomposed upon contact with NaAc. Therefore, this study utilizes the decomposition properties of NaAc to provide an efficient and environmentally friendly route for removing AlN and extracting Al from SAD.

Keywords: secondary aluminum dross; waste sodium acetate; aluminum extraction; phase transformation; Na deconstruction

1. Introduction

Secondary aluminum dross (SAD), which contains the reactive component AlN and a considerable amount of alumina, is a hazardous waste generated by metallic Al production and processing industries [1–2]. In general, SAD is the residue produced after metallic Al is extracted from primary aluminum dross, consisting of 40wt%–60wt% Al_2O_3, 10wt%–30wt% AlN, 5wt%–15wt% salts and other components [3–4]. In recent years, the world aluminum industry experienced steady growth, with annual output of 70.58 million tons in 2023; that is, 0.44–0.71 million tons of SAD was generated (6.3–10 kg SAD per ton of Al electrolytic production) [5–6], theoretically containing 44–213 thousand tons of AlN, which enables hydrolysis to produce environmentally hazardous NH_3 and more than 0.23 million tons of potentially recyclable Al_2O_3 [7–8]. Therefore, a feasible process of efficiently extracting Al while fully removing AlN is of great significance for SAD disposal.

Currently employed methods for decomposing AlN and extracting Al from SAD mainly include hydrometallurgical and pyrometallurgical routes [9]. In hydrometallurgy, Al species react directly with concentrated acid or alkali solutions. The hydrolysis of AlN to bayerite and pseudo-boehmite can proceed spontaneously and can be accelerated by increasing temperature [10–11]. Silica aluminate precipitates formed in hydrolysis side reactions could enhance nitrogen removal efficiency, decreasing residual nitrogen content to 0.39wt% [12]. Furthermore, Al species, including metallic Al, AlN, and $MgAl_2O_4$, in SAD could be converted into Al^{3+} or $[Al(OH)_4]^-$ through a reaction with concentrated acid or alkali, and subsequent pH adjustment leads to the precipitation of the products as $Al(OH)_3$. Corundums and spinels inhibit the transformation of aluminum, leading to the 40% extraction efficiency of alkali leaching [13]. Consequently, the application of hydrometallurgical methods is limited because of the need for ammonia treatment and substantial quantities of concentrated acids or alkalis.

In pyrometallurgical processes, the porous structure of AlN surface oxide layers facilitates AlN removal through high-temperature oxidation. AlN removal efficiency could reach up to 90.86% after 180 min of sintering at 1200°C [14]. Synergistically treating hazardous waste, such as fly ash and pickling sludge, through heat treatment ensures the removal of AlN, the fixation of F and heavy metals, and the volatilization of Cl [15–17]. Additionally, alkaline additives were added to transform Al species into soluble phases $NaAlO_2$ and $12CaO\cdot7Al_2O_3$, and then Al was recovered through leaching

✉ Corresponding author: Nengwu Zhu E-mail: nwzhu@scut.edu.cn
© University of Science and Technology Beijing 2025

and carbonation decomposition [18]. This process was extensively used in the extraction of Al from tailings and slags, exhibiting remarkable efficiency for SAD [19–20]. When exogenous Na_2CO_3 was added to SAD and sintered at 1150°C for 60 min, the AlN removal and Al leaching efficiency increased to 98.93% and 90.79%, respectively [1]. The efficiency of pyrometry in removing hazardous substances and extracting aluminum has its application value for SAD disposal and has a low environmental impact [21]. Thermal treatment for SAD mainly concentrates on high-temperature sections that exceed 1000°C. Applying this method to industrial processes is difficult because of expensive additives and large energy consumption. Therefore, finding cheap alternative additives and reducing costs are important.

Waste sodium acetate (WSA), which contains up to 76.6wt% NaAc, is a hazardous waste generated by the pesticide production industry [22–23]. It releases heat and generates basic components during NaAc decomposition, demonstrating potential application value in the thermal treatment of SAD [24]. Thus, the co-sintering of WSA and SAD would not only facilitate their disposal but also enable the full utilization of NaAc in WSA for AlN decomposition and Al extraction. In this study, the co-sintering of SAD with WSA was proposed to promote AlN decomposition and Al species transformation. First, the effects of sintering conditions on AlN decomposition and Al extraction were investigated using a NaAc reagent and SAD. Then, the effectiveness and feasibility of the method were demonstrated using a typical WSA sample and SAD. Finally, the transformation mechanism of Al species during sintering with NaAc action was clarified. This study could provide novel insights into the utilization of SAD and WSA.

2. Experimental

2.1. Samples and chemicals

SAD and WSA were provided by a metal product plant and a pesticide plant in Guangdong Province, respectively. The raw samples are shown in Fig. S1. Both samples were homogenized, dried, and passed through a 30-mesh sieve for the experiment. The chemical reagents (NaAc, NaOH, HNO_3, $HClO_4$, and HF) used in this study were of analytical grade and provided by Aladdin Chemical Co., Ltd. (Shanghai, China). The chemical composition of the raw samples is listed in Table 1, and the main mineral composition is shown in Fig. 1.

2.2. AlN removal and aluminum extraction experiments

Thermal experiments were conducted in a sintering furnace under air atmosphere (Fig. S2). First, 10.0 g of SAD was thoroughly mixed with NaAc in mass ratios of 1.0, 1.1, 1.2, and 1.3. Subsequently, graphite crucibles containing the mixed samples were placed in a sintering furnace for thermal treatment at different temperatures (750, 800, 850, 900, and 950°C) and varying reaction times (15, 30, 45, 60, 75, and 90 min). The SAD–WSA mixtures and the control without NaAc were sintered under optimal conditions. Secondary ash was the particulate by-product generated during sintering and was collected with an ash collector prior to gas treatment. The sintering product and secondary ash were collected and crushed using an agate mortar and then stored in a drying

Table 1. Chemical composition of the raw samples

Raw SAD				Raw WSA	
Element	Content / wt%	Heavy metal	Content / (mg·kg^{-1})	Element	Content / (mg·kg^{-1})
Al	37.37	Cu	1080	Na	189205.4
Mg	4.62	Ni	101	S	1325.6
Si	3.68	Zn	1260	K	80.6
Na	3.08	Cr	305	Ca	42.9
F	2.04	Pb	147	Fe	20.9
Cl	3.56	Cd	<50	Si	6.2
N	1.49				

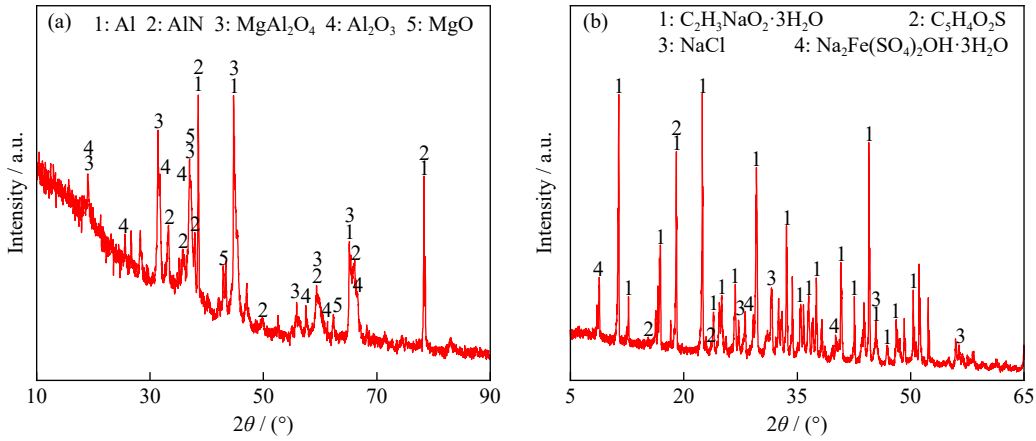

Fig. 1. XRD patterns of (a) raw SAD and (b) raw WSA.

vessel. They were mixed thoroughly, and sample quartering was performed to ensure homogeneity. The determination methods for AlN and heavy metals content are described in Texts S1 and S2.

The sintered product was leached with dilute NaOH solution for aluminum extraction. The sintered product (2.0 g) was mixed with 20.0 mL of 60 g·L^{-1} NaOH solution in a conical flask, which was then placed in a water bath. The temperature was maintained at 90°C for 60 min. The leaching residues were filtered and rinsed three times with boiling water, and the resulting leaching solution was diluted to 200 mL for subsequent analysis.

2.3. Analysis and calculations

The mineral phases of sintering products were detected through X-ray diffraction (XRD; D 8 Advance, Germany), and the NH_4^+ concentration of the absorbent solution was tested with an ultraviolet (UV) spectrophotometer (UV-2600, Japan). X-ray photoelectron spectroscopy (XPS; K-Alpha+, England) analysis was performed, and an Al K_α X-ray source was used for excitation. C 1s peaks at a binding energy of 284.8 eV were used for calibration. The concentration of Al was detected using an inductively coupled plasma-optical emission spectrometry instrument (Agilent ICP 730, USA), and the concentrations of heavy metals, such as Cu, Pb, Zn, Ni, Cr, and Cd, were analyzed using atomic absorption spectroscopy (Shimadzu AA 6880, Japan). The specific surface areas of the samples were tested using a Brunauer–Emmett–Teller (BET) system (Micrometrics ASAP 2460, USA). The thermal reaction was analyzed using a thermogravimetric-differential thermal analysis (TG–DTA) instrument (Mettler TG–DSC 3+, Switzerland). The morphology of the samples was characterized using a field-emission scanning electron microscopy system and energy dispersive spectrometer (SEM–EDS; Zeiss Ultra 55, Germany).

To quantify the removal effects of AlN or heavy metals (Cu, Pb, Zn, and Cr), the removal efficiency (η_1) was defined as the percentage of AlN or heavy metals removed through sintering, as shown in Eq. (1).

$$\eta_1 = \frac{C_0 \times M_0 - C_1 \times M_1}{C_0 \times M_0} \times 100\% \quad (1)$$

where C_0 is the content of AlN or heavy metals in the raw SAD (mg·kg^{-1}), M_0 is the mass of the raw SAD (g), C_1 is the content of AlN or heavy metals in the sintering product (mg·kg^{-1}), and M_1 is the mass of the sintering product (g).

The efficiency of the Al leaching process (η_{Al}) was calculated using Eq. (2). It was expressed as a percentage of the amount of Al present in the leaching solution as compared with the total amount of Al in the raw SAD.

$$\eta_{Al} = \frac{L_1 \times V_1 \times M_1}{L_0 \times M_0 \times M_2} \times 100\% \quad (2)$$

where L_0 is the content of Al in the raw SAD (mg·kg^{-1}), M_0 is the mass of the raw SAD (g), M_2 is the mass of the sample that participated in the leaching process (g), L_1 is the concentration of Al in the leaching solution (mg·L^{-1}), V_1 is the volume of leaching solution (mL), and M_1 is the mass of the sintering product (g). All experiments were repeated twice, and the results were expressed as mean values.

3. Results and discussion

3.1. Theoretical analysis of sintering and leaching processes

The reaction between NaAc and SAD was clarified through TG–DTA (Fig. 2(a)). The process could be divided into three stages: (1) From room temperature to approximately 300°C, mass loss initially increased rapidly, and the rate gradually decelerated. These effects were mainly caused by the volatilization of attached water in NaAc and heat decomposition of $Al(OH)_3$ in SAD. In addition, the raw SAD mass increased to 100.6% at 213.5°C mainly through metallic Al oxidation that produced Al_2O_3 (Eq. (3)). (2) From 300 to 500°C, co-sintering sample quality decreased from 94.6% to 80.1% as temperature increased from 323.7 to 494.1°C, indicating NaAc decomposed into Na_2CO_3. The huge exothermic peak at 461.1°C demonstrated that the reaction released a large amount of heat (Eq. (4)) [25]. (3) From 500 to 1000°C, the weight of the raw NaAc sample decreased rapidly above 849.1°C, and only 28.7% was produced at 1000°C because of the decomposition of Na_2CO_3 to Na_2O (Eq. (5)). The raw SAD sample showed a slight mass increase at 683.5°C and was accompanied by 713.9°C and 920.1°C endothermic peaks. AlN was oxidized to Al_2O_3 (Eq. (6)) [26]. The mixture mass decreased gradually, and a large endothermic peak appeared at 640.0, 698.4, and 918.9°C. The pyrolysis of Na_2CO_3 produced Na_2O and caused massive endothermic reactions with SAD components (Eqs. (7)–(11)), possibly generating MgO, $NaAlO_2$, $NaAl_{11}O_{17}$, $Na_{1.75}Al_{1.75}Si_{0.25}O_4$, and $Na_{1.95}Al_{1.95}Si_{0.05}O_4$ [27]. The Gibbs free energy varied with temperature during sintering, as shown in Fig. 2(b). As the temperature increased, the Gibbs free energy associated with Eqs. (9)–(11) notably decreased.

$$4Al(s) + 3O_2(g) = 2Al_2O_3(s) \quad (3)$$

$$2CH_3COONa(s) + 4O_2(g) = Na_2CO_3(s) + 3CO_2(g) + 3H_2O(g) \quad (4)$$

$$Na_2CO_3(s) = Na_2O(s) + CO_2(g) \quad (5)$$

$$4AlN(s) + 3O_2(g) = 2Al_2O_3(s) + 2N_2(g) \quad (6)$$

$$MgAl_2O_4(s) + Na_2CO_3(s) = MgO(s) + 2NaAlO_2(s) + CO_2(g) \quad (7)$$

$$Al_2O_3(s) + Na_2CO_3(s) = 2NaAlO_2(s) + CO_2(g) \quad (8)$$

$$11Al_2O_3(s) + Na_2CO_3(s) = 2NaAl_{11}O_{17}(s) + CO_2(g) \quad (9)$$

$$1.75Al_2O_3(s) + 1.75Na_2CO_3(s) + 0.5SiO_2(s) = 2Na_{1.75}Al_{1.75}Si_{0.25}O_4(s) + 1.75CO_2(g) \quad (10)$$

$$1.95Al_2O_3(s) + 1.95Na_2CO_3(s) + 0.1SiO_2(s) = 2Na_{1.95}Al_{1.95}Si_{0.05}O_4(s) + 1.95CO_2(g) \quad (11)$$

The existence forms and transformation mechanisms of metal phases in the solutions at varying pH levels were in-

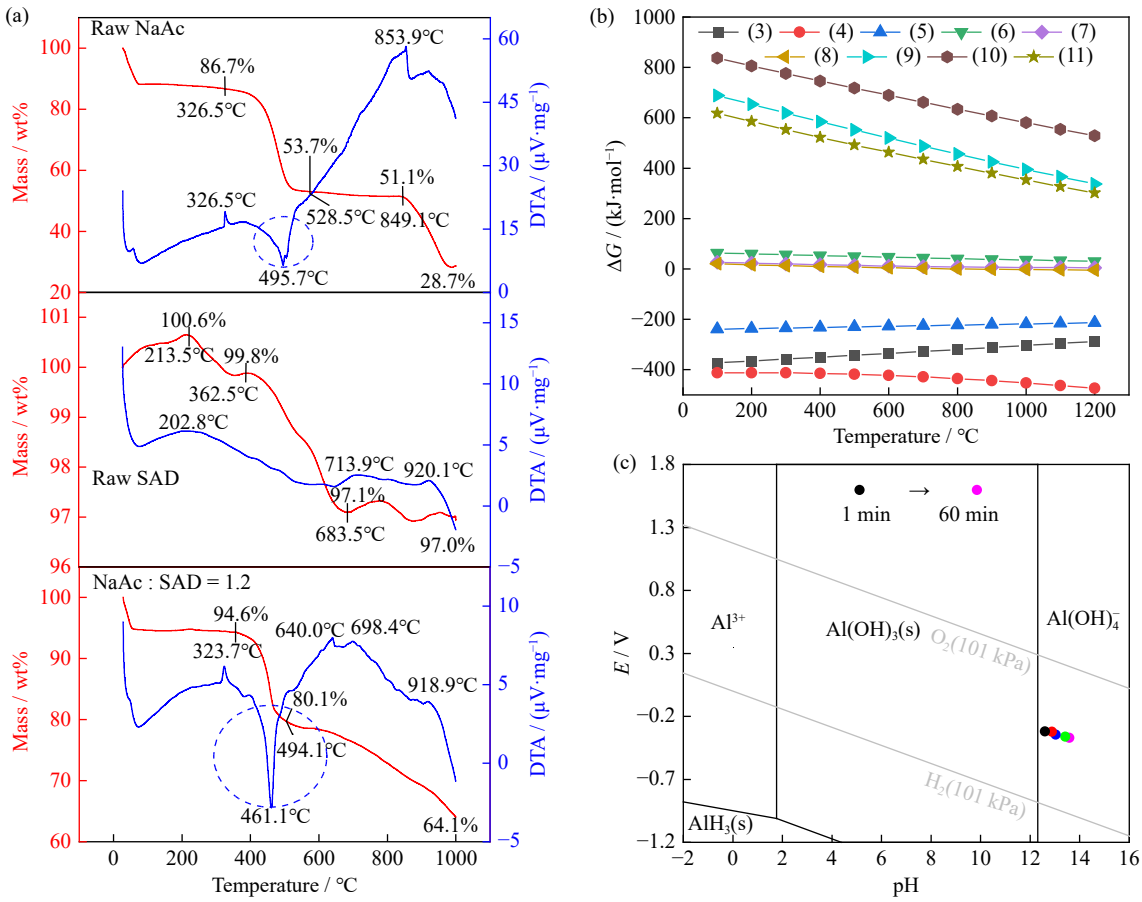

Fig. 2. (a) TG–DTA curves of different samples; (b) Gibbs free energy varying with temperature during sintering; (c) *E*–pH diagram of the Al–H_2O system under the conditions of 90°C and 101 kPa at 1, 15, 30, 45, and 60 min.

vestigated with an *E*–pH diagram (*E* means electric potential) [28]. When the pH ranged from 1.76 to 12.31, Al precipitated out in the form of $Al(OH)_3$ (Fig. 2(c)). Conversely, when the pH exceeded 12.31, Al remained stable in the form of $[Al(OH)_4]^-$. After the product was sintered with 60 g·L^{-1} NaOH, the pH of the solution gradually increased to 13.58, suggesting that the Al within the product was effectively extracted through leaching.

In summary, the phase transformation of Al species primarily occurred within a temperature range of 600–950°C. Furthermore, the thermal treatment temperature decreased because of the massively exothermic reaction that occurred at 400–500°C. Meanwhile, leaching enabled an efficient extraction of Al from the sintering product.

3.2. AlN removal process of SAD

In the UV results, the AlN content of raw SAD was up to 4.35wt%. The decomposition characteristics of AlN in SAD in the presence of NaAc were investigated with a sintering experiment.

Effect of sintering temperature. The impact of sintering temperature was investigated with a mass ratio of 1.1 between NaAc and SAD, and the sintering time was 60 min (Fig. 3(a)). The removal efficiency of AlN continued to increase with the sintering temperature increasing from 750 to 950°C, and the content of AlN in the product decreased accordingly. The increase in temperature accelerated the reaction of AlN [29]. Notably, the AlN content was 0.20wt%, and the removal efficiency reached 93.15% at 850°C, which is significantly lower than the requirement in the standard T/CSTM 00905—2023 (N content less than 0.2wt%). Although higher removal efficiency can be achieved above 900°C, it also means more energy consumption. Therefore, 850°C was the recommended temperature.

Effect of NaAc mass ratio. The effect of NaAc mass ratio ranging from 1.0 to 1.3 on AlN removal was studied during sintering at 850°C for 60 min (Fig. 3(b)). As the mass ratio of NaAc increased to 1.3, the removal efficiency of AlN gradually increased and reached a maximum of 94.32%, and the growth stabilized when the ratio exceeded 1.2. In the control experiment without NaAc, the AlN content and removal efficiency were only 1.24wt% and 67.60%, respectively. NaAc promoted AlN removal, possibly by disrupting the Al_2O_3 membrane and allowing the internal AlN to react further [14]. Overall, the AlN removal efficiency reached 94.19% at a ratio of 1.2. The increase in removal efficiency was not readily apparent when the ratio was increased from 1.2 to 1.3. Therefore, the ideal ratio for SAD disposal was 1.2.

Effect of sintering time. The influence of sintering time on the removal of AlN was investigated under optimal sintering temperature and NaAc mass ratio conditions. The removal efficiency of AlN reached as high as 89.30% at 30 min and gradually increased as the time extended to 75 min (Fig. 3(c)). As the residual AlN continuously participated in the re-

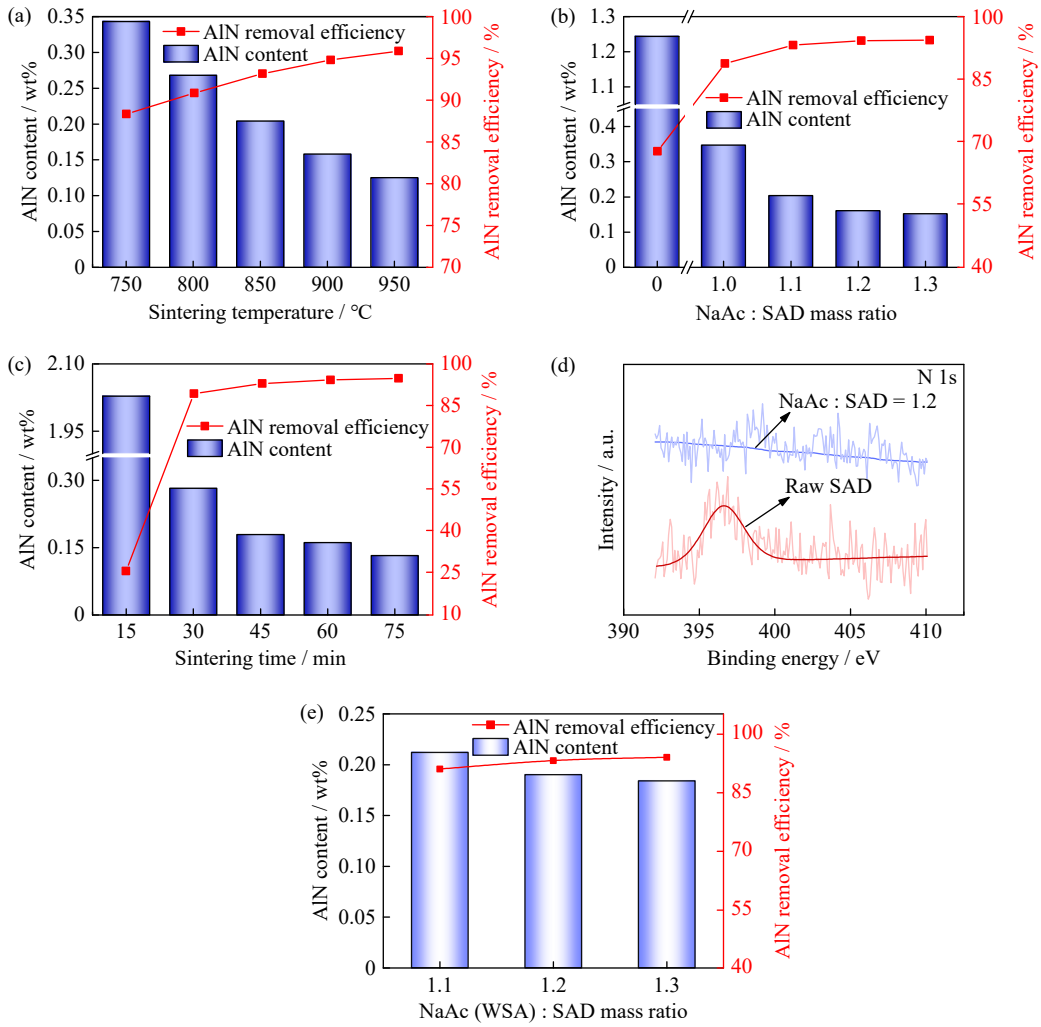

Fig. 3. (a–c) AlN content and removal efficiency of SAD in the NaAc co-sintering system: (a) sintering temperature (1.1:1 NaAc-to-SAD mass ratio and 60 min); (b) mass ratio of NaAc and SAD (850°C and 60 min); (c) sintering time (1.2:1 NaAc-to-SAD mass ratio and 850°C). (d) XPS spectra of the raw SAD and sintering product in a ratio of 1.2 (N 1s); (e) AlN content and removal efficiency in the WSA and SAD co-sintering system.

action, the removal efficiency reached 94.19% at 60 min, and the increase from 60 to 75 min was slight. In order to achieve as complete removal of AlN as possible, and improve the economic benefits of the overall process, the recommended sintering time was 60 min.

In summary, the preferred conditions were a sintering temperature of 850°C, NaAc–SAD mass ratio of 1.2, and time of 60 min. Under these conditions, the AlN content was reduced to 0.16wt%, and the removal efficiency reached 94.19%. Under the same testing conditions, the disappearance of the N characteristic peak in the XPS analysis results indicated that the content of AlN in the product may have fallen below the detection limit of the equipment (Fig. 3(d)). The large reduction in AlN content was consistent with the experimental results.

Meanwhile, the effectiveness of the reaction system was verified using WSA samples, and the results are shown in Fig. 3(e). When the mass ratio of NaAc to SAD was adjusted to 1.2 through the addition of WSA, the removal efficiency of AlN increased to 93.19%， and the efficiency increased by 37.86% relative to that of the control. However, a further increase in the amount of WSA did not substantially enhance removal efficiency, indicating that a plateau was reached. Nevertheless, WSA is a valid additive that promotes AlN decomposition.

3.3. Aluminum extraction from sintering product

The Al species in SAD were converted into a leachable state through sintering and extracted as $[Al(OH)_4]^-$ through leaching [18]. Therefore, the effects of sintering parameters on the transformation of Al species were considered, and the results are shown in Fig. 4.

Effect of sintering temperature. The leaching efficiency of Al reached a maximum value of 82.94% at 850°C and then decreased to 49.22% as the temperature increased to 950°C (Fig. 4(a)). NaAc decomposition is the possible reason that the sintering temperature for Al extraction should be decreased. The low efficiency below 800°C was due to the incomplete phase transformation of the Al species, whereas the decrease in leaching efficiency above 900°C might be related to the volatilization of Na (Fig. 4(b)). Consequently, a sintering temperature of 850°C was recommended.

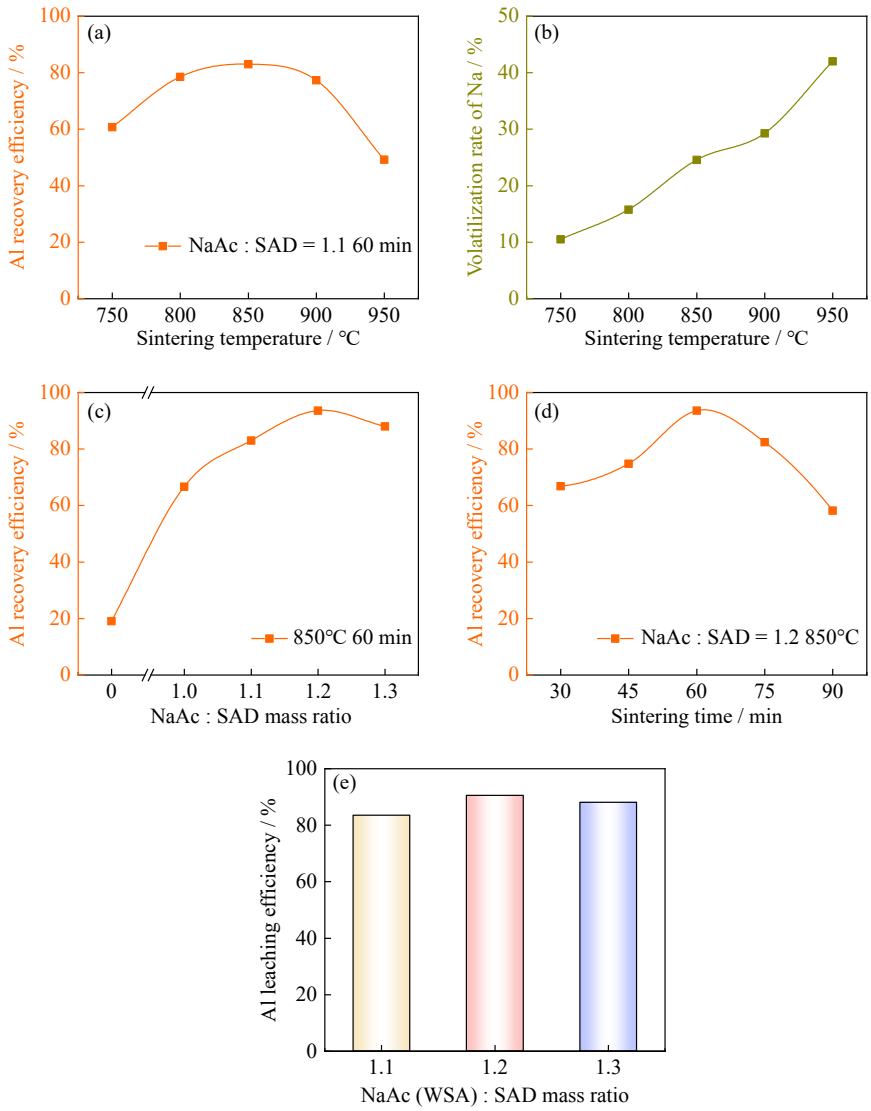

Fig. 4. Al leaching efficiency at different sintering conditions: (a) sintering temperatures, (c) mass ratios between NaAc and SAD, and (d) sintering times; (b) Na volatilization rates of the sintering products at different sintering temperatures; (e) Al leaching efficiency in WSA and SAD co-sintering system.

Effect of NaAc mass ratio. Leaching efficiency was only 19.04% in the control group without NaAc. The rate reached 66.68% when the mass ratio was 1.0 and increased to 93.55% as the ratio was adjusted to 1.2 (Fig. 4(c)). NaAc induced the transformation of Al species into a leachable phase, whereas Na loss prevented the full conversion of aluminum components. NaAc facilitated thorough conversion and improved leaching efficiency. However, leaching efficiency decreased to 87.94% when the ratio was 1.3. The reason could be excessive sodium causing side reactions and generating non-leachable species. Therefore, a 1.2:1 NaAc–SAD mas ratio was used in exploring the effect of time.

Effect of sintering time. The leaching efficiency was only 66.77% when the sintering time was 30 min and gradually increased to its maximum value (93.55%) as the time was extended to 60 min. However, when the time was further extended to 90 min, the leaching efficiency decreased to 58.17% (Fig. 4(d)). The reaction for the production of leachable phases was completed at 60 min, and additional side reactions occurred when the time was further extended. Therefore, 60 min was considered the optimal sintering time.

After the sintering conditions were evaluated, the optimal parameters were established: the NaAc–SAD mass ratio of 1.2, sintering temperature of 850°C, and sintering time of 60 min. Under these optimal conditions, the Al leaching efficiency reached 93.55%. Additionally, the co-sintering system utilizing WSA and SAD exhibited impressive performance. Al leaching efficiency in the co-sintering system is shown in Fig. 4(e). The Al leaching efficiency reached a maximum value of 90.49% after the WSA was added, with a mass ratio of NaAc to SAD of 1.2. Compared with the efficiency of the control without NaAc, the efficiency represented a significant improvement of 375.26%. WSA can serve as an effective additive for the extraction of Al from SAD.

3.4. Mechanism of NaAc promoting AlN decomposition and aluminum extraction

3.4.1. Existential pattern of main Al species in SAD

The principal phase composition and distribution pattern of SAD were elucidated through multiple analyses. The XRD

results showed that the main Al species in SAD were metallic Al, AlN, Al_2O_3, and $MgAl_2O_4$ (Fig. 1(a)). The distribution of the main elements in SAD was clarified through SEM–EDS analysis (Fig. 5(a)). The results depicted that the surfaces of the particles were mainly composed of Al and O, and N and Mg were scattered on the surfaces. The similar distribution patterns of N, Al, and O elements shown in the yellow circle indicated that AlN was diffusely distributed within the Al_2O_3 phase. Conversely, the relatively uniform distribution of Mg suggested the random distribution of $MgAl_2O_4$. Furthermore, the distribution pattern of internal AlN was clarified through XPS etching analysis (Fig. 5(b)). The N content on the surface of a SAD particle was only 0.65at% but increased to 1.82at% at a depth of 60 nm. This result indicated that AlN was predominantly present within the SAD particles. The presence of stable Al_2O_3 and $MgAl_2O_4$ not only restricts the extraction of Al but also inhibits the thorough removal of internal AlN.

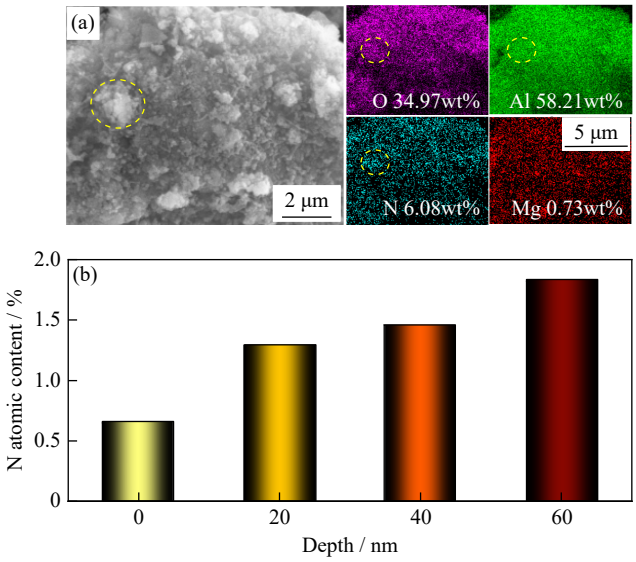

Fig. 5. Distribution characteristic of main elements in SAD: (a) SEM–EDS images; (b) N atomic content at different depths of the SAD particle.

3.4.2. Phase transformation of the Al species

The transformation pattern of Al species during sintering was clarified through XRD and XPS tests (Fig. 6). The peaks corresponding to AlN and Al were present only at 750°C and disappeared at temperatures above 800°C, whereas the peak intensities of the $Na_{1.95}Al_{1.95}Si_{0.05}O_4$ phase increased gradually (Fig. 6(a)). When SiO_2 participated in the conversion reaction of Al_2O_3, the $Na_{1.95}Al_{1.95}Si_{0.05}O_4$ phase formed [30]. As the temperature continued to increase, $Na_{1.95}Al_{1.95}Si_{0.05}O_4$ was converted into $Na_{1.75}Al_{1.75}Si_{0.25}O_4$ and $NaAl_{11}O_{17}$. The possible explanation for this reaction is that a high temperature triggers the volatilization of Na (Fig. 4(b)). Simultaneously, the $MgAl_2O_4$ side product produced by MgO and Al_2O_3 caused a decrease in MgO peak intensity and an increase in $MgAl_2O_4$ peak intensity. Overall, the transformation of Al species into the soluble state $Na_{1.95}Al_{1.95}Si_{0.05}O_4$ enhanced the extraction of Al. However, insoluble components, including $NaAl_{11}O_{17}$, Al_2O_3, and $MgAl_2O_4$, impeded the leaching process.

The phase composition of the sintering products at different mass ratios between NaAc and SAD is shown in Fig. 6(b). The control experiment revealed the presence of trace amounts of AlN, and most of the Al species were present in the form of Al_2O_3 and $MgAl_2O_4$. As the ratio was raised to 1.0, Al species in the product were primarily present as $Na_{1.75}Al_{1.75}Si_{0.25}O_4$, and a small amount of unreacted Al_2O_3 remained. The addition of NaAc facilitated the transformation of Al species. As the ratio was further increased, nearly all the Al species were transformed into $Na_{1.95}Al_{1.95}Si_{0.05}O_4$. Furthermore, as the ratio increased to 1.2, the peak intensity of $MgAl_2O_4$ gradually diminished, whereas the MgO peak intensity increased. This result indicated that NaAc had a considerable effect on the transformation of $MgAl_2O_4$ and $Na_{1.75}Al_{1.75}Si_{0.25}O_4$ to MgO and $Na_{1.95}Al_{1.95}Si_{0.05}O_4$.

The phase composition of the sintering products at different sintering times is depicted in Fig. 6(c). When the sintering time was limited to 30 min, some unreacted Al_2O_3 and $MgAl_2O_4$ remained in the products, inhibiting Al extraction. The main components of Al in the products primarily transformed into $Na_{1.75}Al_{1.75}Si_{0.25}O_4$ and $Na_{1.95}Al_{1.95}Si_{0.05}O_4$. As the sintering time was extended, the proportion of $Na_{1.95}Al_{1.95}Si_{0.05}O_4$ increased.

The XPS spectrum provided further insights into the role of Na in the sintering process. Initially, Al–Al (72.46 eV), Al–N (73.53 eV), and Al–O–Al (74.25 eV, 74.82 eV) bonds were observed, indicating the presence of metallic Al, AlN, Al_2O_3, and $MgAl_2O_4$ [31] (Fig. 6(d)). However, Al and AlN were transformed into Al_2O_3, and the primary bonding form of Al shifted to Al–O–Al in the control without NaAc (Fig. 6(e)). The content of O element in the product increased considerably during the oxidation of metallic Al and AlN (Fig. S3). Notably, the Al species mainly existed in a single form when the ratio was 1.2, indicating an Al–O–Na bond (Fig. 6(f)). Therefore, AlN was converted into the $Na_{1.95}Al_{1.95}Si_{0.05}O_4$ phase together with other aluminum com-

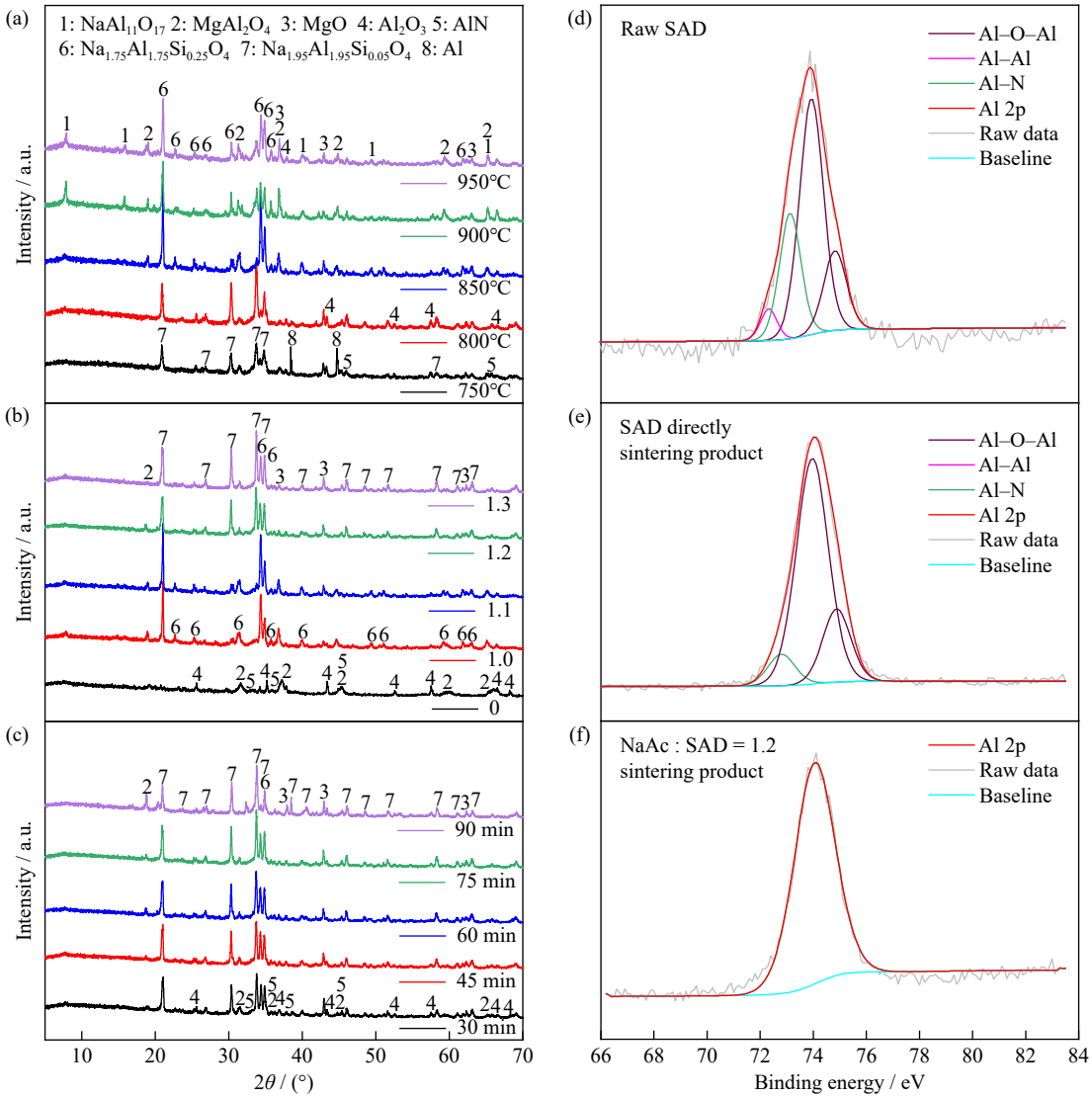

Fig. 6. XRD patterns of sintering products under different conditions: (a) sintering temperature; (b) the mass ratio of NaAc to SAD; (c) sintering time. Al 2p XPS spectra of different samples: (d) raw SAD; (e) SAD directly sintered product without NaAc; (f) NaAc : SAD = 1.2 sintering product.

ponents under the action of NaAc.

The transition of Al species affects internal heavy metal migration. TG–DTA results showed that the main transformation temperature of the Al species was 600–950°C. Zn, Pb, and Cd exhibited high removal efficiency at this temperature [32–33]. However, SAD exhibited only 35.66% and 40.40% removal efficiency for Zn and Pb, respectively, under the no NaAc addition condition, but the removal efficiency increased rapidly to 45.28% and 100% when the mass ratio of NaAc and SAD was adjusted to 1.2 (Fig. 7(a)). This result indicated that the wrapped heavy metals were released because Na destroyed the stability of Al species at high temperatures [34]. The XRD patterns of secondary ash showed that heavy metals Zn, Cr, and Pb in SAD volatilized into secondary ash in the form of fluorides and chlorides (Fig. 7(b)). Meanwhile, the intensity of the main absorption peak of the secondary ash was increased by the action of NaAc.

In summary, Al species, including metallic Al, AlN, Al_2O_3, and $MgAl_2O_4$, were primarily transformed into $Na_{1.95}Al_{1.95}Si_{0.05}O_4$. The smallest insoluble Al species of $NaAl_{11}O_{17}$ and Al_2O_3 peaks were observed at a ratio of 1.2 after sintering at 850°C for 60 min, consistent with the maximum Al leaching efficiency. The process of removing heavy metals, F, and Cl was greatly enhanced by NaAc.

3.4.3. Structural characteristics of sintering products

The morphology of the sintering products under the recommended conditions is shown in Fig. 8(a). The relative content of Al in the product decreased to 22.79wt%, whereas the content of Na notably surged to 26.36wt%; thus, the mass ratio between Na and Al approached 1:1. Meanwhile, SAD particles transformed into loose porous particles and sheet structures after sintering with NaAc. The transformation indicated that NaAc effectively disrupted the relatively stable structure of SAD and exposed the internal species, thereby facilitating the deep removal of AlN encapsulated by Al_2O_3. The microstructure of the sintering products was further investigated through BET analysis (Fig. 8(b)), and the surface area increased from 0.0608 to 0.2202 $m^2 \cdot g^{-1}$ as the ratio increased from 1.0 to 1.2. However, a further increase in the NaAc ratio led to a decrease in the surface area. Similarly,

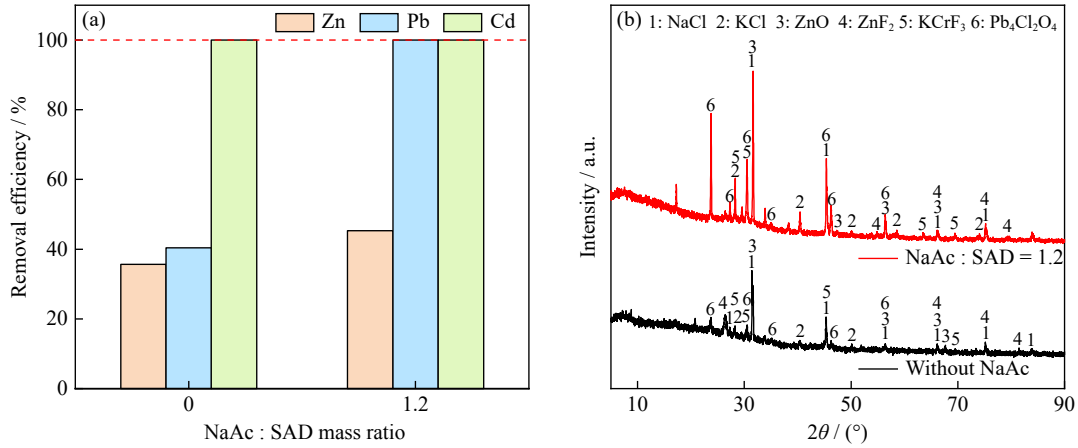

Fig. 7. (a) Removal efficiency of heavy metals; (b) XRD pattern of secondary ash.

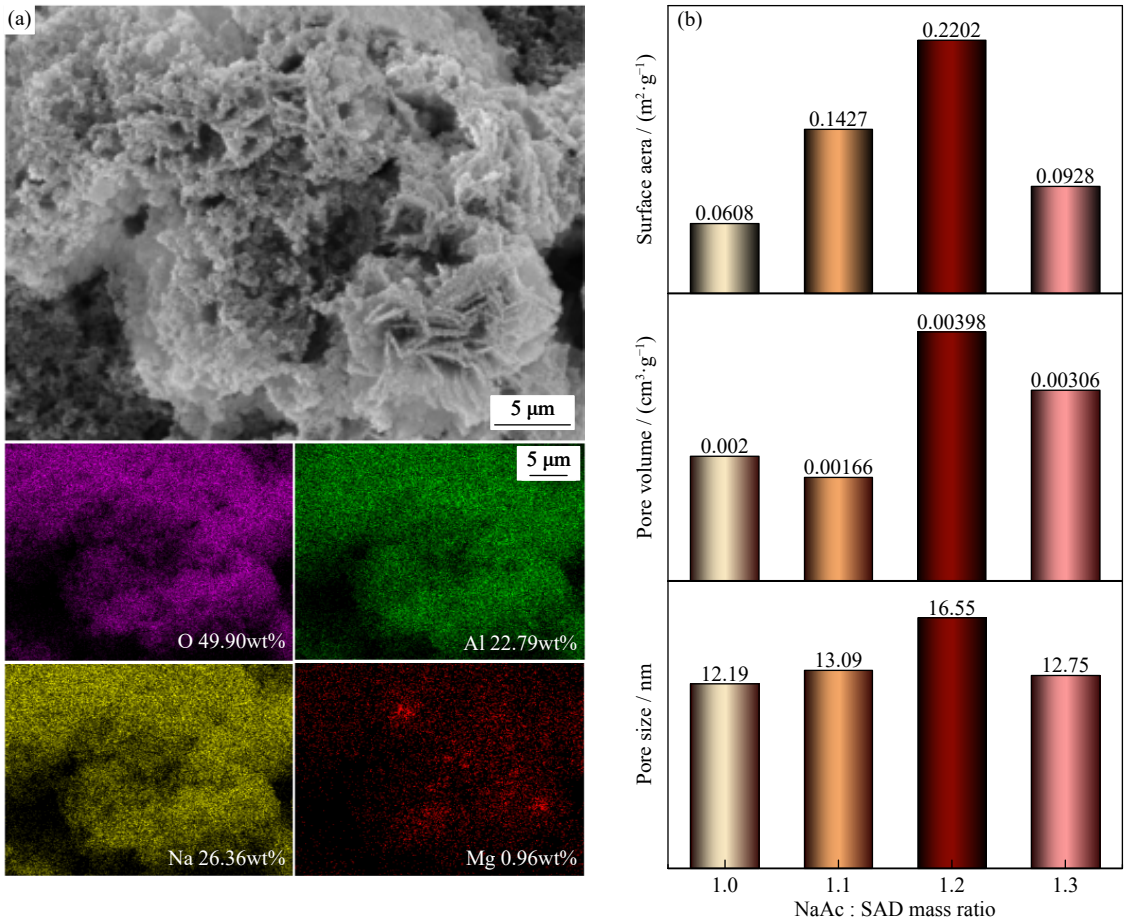

Fig. 8. Structural characteristics of sintered products: (a) SEM–EDS analysis of NaAc : SAD = 1.2 co-sintering product; (b) physical parameters of sintering products at different ratios of NaAc.

pore volume and diameter reached their peak values of 0.00398 $cm^3 \cdot g^{-1}$ and 16.55 nm at a ratio of 1.2, respectively. The highest porosity of the sintering product was obtained at 1.2, facilitating gas and solid phase reactions. Moreover, the heavy metal and F leaching toxicity of the sintering products was assessed, and the outcomes were notably below the regulatory threshold specified in GB 5085.3—2007 (Table 2). SAD was successfully transformed into general solid waste and became suitable for further utilization.

In summary, the mechanism of Al species transformation induced by NaAc to promote AlN decomposition and Al extraction can be attributed to the following aspects (Fig. 9). The interaction of NaAc with SAD particles disrupted the compact structure of Al_2O_3, revealing interior components, such as AlN, heavy metals, F, and Cl. Additionally, the loosened structure resulting from these reactions not only promoted reactions between Al and Na and converted Al into more soluble phases but also accelerated the dissolution of $Na_{1.95}Al_{1.95}Si_{0.05}O_4$.

3.5. Implications

Alkali additives facilitate the removal of AlN and Al from

Table 2. Heavy metals, F, and Cl leaching toxicity of sintering products (mg·L^{-1})

Sintering products	Cu	Ni	Zn	Cr	Pb	Cd	F	Cl
NaAc : SAD = 1.0	ND	ND	0.0037	7.2519	0.0019	ND	2.06	3.95
NaAc : SAD = 1.1	0.0068	0.0012	0.0071	6.9098	0.0016	0.0039	1.58	2.67
NaAc : SAD = 1.2	0.0086	ND	0.0143	2.0093	0.0019	0.0057	0.99	1.87
NaAc : SAD = 1.3	0.0147	ND	0.0304	3.1790	0.0037	0.0035	0.64	1.48
Regulatory limit of GB 5085.3—2007	100	5	100	15	5	1	100	

Note: ND—Not detected.

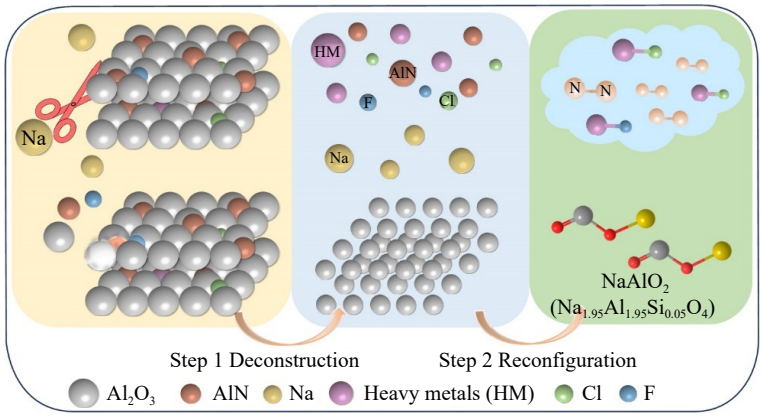

Fig. 9. Mechanism of Na-induced Al species transformation and AlN decomposition.

SAD and increase the transformation potential of Al species [35–36], but the high cost of additives and their high energy consumption restrict their industrial application. In this work, WSA efficiently eliminated AlN and transformed Al species, facilitating aluminum recovery (Table 3). Moreover, it not only facilitated the disposal of two hazardous waste materials but also minimized alkali consumption and energy expenditure through the action of NaAc.

Economic benefits can be enhanced by considering the resource utilization of leaching residues and leaching solutions. Si (10.9wt%) and Mg (1.73wt%) were detected in leaching residue [39]. Further work could combine the leaching residue with industrial solid waste to prepare high-value ceramic glass [40] and zeolite-A and zeolite-X [41] and to achieve the full resource utilization of SAD. Concurrently, a leaching solution contains high concentrations of $[Al(OH)_4]^-$ and NaOH. Through the reuse of leaching solutions, Al and alkali can be continuously recovered with SAD and WSA. Additionally, an off-gas circulation and purification device is required for technological application [42]. Although NaAc can inhibit the formation of NO_x, exhaust gas still needs to be detected and evaluated [43].

Table 3. Evaluation of various processes for decomposing AlN and extracting Al from SAD

Method	Reagents	Evaluation	Reference
Directly sintering		Remove 90.86% AlN sintering at 1200°C for 180 min	[37]
Sodium carbonate roasting	Na_2CO_3/SAD mass ratio of 0.6	Remove 91.32% AlN roasting at 1000°C for 240 min	[38]
Combined dry pressing and alkaline roasting	Na_2CO_3/Al_2O_3 molar ratio of 1.3	Remove 98.93% AlN and extract 90.79% Al sintering at 1150°C for 60 min	[1]
Calcification roasting	Calcification coefficient of 1.05	Remove 99% AlN and extract 87.89% Al roasting at 1300°C for 30 min	[35]
Alkaline roasting	$NaOH/Al_2O_3$ molar ratio of 1.4	Extract 86.7% Al roasting at 1000°C for 40 min	[19]
WSA co-sintering	NaAc/SAD mass ratio of 1.2	Remove 93.19% AlN and extract 90.49% Al sintering at 850°C for 60 min	This study

4. Conclusion

A co-sintering system of SAD and WSA was proposed to efficiently decompose AlN and simultaneously extract Al. The decomposition of AlN and transformation of Al species into leachable phases were facilitated by NaAc. When SAD was mixed with WSA in NaAc and SAD mass ratio of 1.2 and sintered at 850°C for 60 min, the hazardous AlN content was reduced to 0.16wt%, and the removal efficiency reached 93.19%. Subsequently, Al leaching efficiency of 90.49% was attained through leaching. During sintering, the stable structure of Al species in SAD was disrupted and transformed into the leachable phase $Na_{1.95}Al_{1.95}Si_{0.05}O_4$. The disruption of the Al_2O_3 structure released the encapsulated AlN and induced the deep removal of internal AlN. Through the exothermic combustion of NaAc from 400 to 500°C, the reaction temperature of the system considerably decreased. This work presents an eco-friendly method for efficiently remov-

ing AlN and extracting Al from SAD while considerably reducing alkali consumption and energy expenditure.

Acknowledgements

This study was financially supported by the National Natural Science Foundation of China (No. 22276062) and the Guangdong Science and Technology Program, China (No.2020B121201003).

Conflict of Interest

All authors do not have competing interests to declare.

Supplementary Information

The online version contains supplementary material available at https://doi.org/10.1007/s12613-024-2990-9.

References

[1] H. Lv, M.Z. Xie, Z.G. Wu, *et al*., Effective extraction of the Al element from secondary aluminum dross using a combined dry pressing and alkaline roasting process, *Materials*, 15(2022), No. 16, art. No. 5686.

[2] Z.J. Su, K. Liu, K. Lin, S. Liu, Y.B. Zhang, and T. Jiang, A novel route to denitrify, recover chlorines and prepare premelted refine slag of $12CaO\cdot7Al_2O_3$ ($C_{12}A_7$) from secondary aluminum dross (SAD), *J. Mater. Res. Technol.*, 19(2022), p. 1203.

[3] H.L. Shen, B. Liu, C. Ekberg, and S.G. Zhang, Harmless disposal and resource utilization for secondary aluminum dross: A review, *Sci. Total Environ.*, 760(2021), art. No. 143968.

[4] X.H. Zhu, J.Z. Yang, Y.F. Yang, Q.F. Huang, and T. Liu, Pyrometallurgical process and multipollutant co-conversion for secondary aluminum dross: A review, *J. Mater. Res. Technol.*, 21(2022), p. 1196.

[5] H.K. Yuan, T. Luo, D.K. Zhang, and Q. Wang, Harmless treatment and recycling of secondary aluminum dross: A review, *J. Sustainable Cem. Based Mater.*, 12(2023), No. 11, p. 1460.

[6] Y.S. Tang, L.T. Ma, Z.S. Qiu, W.Z. Yang, B.S. Chen, and Y. Lin, Research on synergistic disposal and high-value utilization of secondary aluminum dross and spent carbon anode, *Process Saf. Environ. Prot.*, 184(2024), p. 1094.

[7] E. David and J. Kopac, Hydrolysis of aluminum dross material to achieve zero hazardous waste, *J. Hazard. Mater.*, 209-210(2012), p. 501.

[8] A. Gil and S.A. Korili, Management and valorization of aluminum saline slags: Current status and future trends, *Chem. Eng. J.*, 289(2016), p. 74.

[9] A. Meshram and K.K. Singh, Recovery of valuable products from hazardous aluminum dross: A review, *Resour. Conserv. Recycl.*, 130(2018), p. 95.

[10] Q. Li, Q. Yang, G.F. Zhang, and Q. Shi, Investigations on the hydrolysis behavior of AlN in the leaching process of secondary aluminum dross, *Hydrometallurgy*, 182(2018), p. 121.

[11] Z.P. Zuo, H. Lv, R.B. Li, F.Q. Liu, and H.L. Zhao, A new approach to recover the valuable elements in black aluminum dross, *Resour. Conserv. Recycl.*, 174(2021), art. No. 105768.

[12] Y.B. Zhang, K. Lin, Z.J. Su, J.M. Xu, and T. Jiang, Self-driven hydrolysis mechanism of secondary aluminum dross (SAD) in the hydrometallurgical process without any additives, *Chem. Eng. J.*, 466(2023), art. No. 143141.

[13] A. Jiménez, V. Rives, M.A. Vicente, and A. Gil, A comparative study of acid and alkaline aluminum extraction valorization procedure for aluminum saline slags, *J. Environ. Chem. Eng.*, 10(2022), No. 3, art. No. 107546.

[14] C.T. Yeh and W.H. Tuan, Oxidation mechanism of aluminum nitride revisited, *J. Adv. Ceram.*, 6(2017), No. 1, p. 27.

[15] H.L. Shen, B. Liu, J.J. Zhang, J. Liu, and S.G. Zhang, Homogeneous reduction for heavy metals from pickling sludge with aluminum nitride from secondary aluminum dross in aluminosilicate melt 'solution' environment, *J. Cleaner Prod.*, 362(2022), art. No. 132358.

[16] J.W. Li, A.G. Jia, X.S. Hou, X.J. Wang, Y.P. Mao, and W.L. Wang, Thermal co-treatment of aluminum dross and municipal solid waste incineration fly ash: Mineral transformation, crusting prevention, detoxification, and low-carbon cementitious material preparation, *J. Environ. Manage.*, 329(2023), art. No. 117090.

[17] H.M. Xie, Z.H. Guo, R. Xu, Y.L. Zhang, and Z. Xu, Synergistic effect of inorganic salt and AlN removal in the secondary aluminum dross during the roasting process, *J. Alloy. Compd.*, 966(2023), art. No. 171518.

[18] J.J. Liu, C.H. Peng, J. Jiang, *et al*., Recovery of iron and aluminum from iron-rich bauxite residue by an integrated phase reconstruction approach, *Sci. Total Environ.*, 904(2023), art. No. 166702.

[19] L.Q. He, L. Shi, Q.Z. Huang, *et al*., Extraction of alumina from aluminum dross by a non-hazardous alkaline sintering process: Dissolution kinetics of alumina and silica from calcined materials, *Sci. Total Environ.*, 777(2021), art. No. 146123.

[20] A.K. Tripathy, S. Mahalik, C.K. Sarangi, B.C. Tripathy, K. Sanjay, and I.N. Bhattacharya, A pyro-hydrometallurgical process for the recovery of alumina from waste aluminium dross, *Miner. Eng.*, 137(2019), p. 181.

[21] L.Y. Xiao, Y. Wang, R.F. Zheng, *et al*., Identification of recycling pathways for secondary aluminum dross with integrated hybrid life cycle assessment, *Resour. Conserv. Recycl.*, 193(2023), art. No. 106987.

[22] S.B. Xi, X.L. Wei, J. Ding, W.L. Wang, and J.F. Lu, The removal of organic contaminants from industrial waste salts by pyrolysis and potential use for energy storage, *J. Cleaner Prod.*, 425(2023), art. No. 138931.

[23] S. Xue, C.M. Wu, Y.H. Wu, J. Chen, and Z.X. Li, Bipolar membrane electrodialysis for treatment of sodium acetate waste residue, *Sep. Purif. Technol.*, 154(2015), p. 193.

[24] S. Cheng, Y. Qiao, J.C. Huang, *et al*., Effects of Ca and Na acetates on nitrogen transformation during sewage sludge pyrolysis, *Proc. Combust. Inst.*, 37(2019), No. 3, p. 2715.

[25] K.A. Kemper and J.E. House, A DSC and IR study of the phase transition in anhydrous sodium acetate, *Thermochim. Acta*, 170(1990), p. 253.

[26] M.Z. Xie, H. Lv, H.L. An, F.Q. Liu, and H.L. Zhao, Effect of alkali doping on the preparation of calcium aluminate by aluminum dross calcification process, *Environ. Technol. Innovation*, 32(2023), art. No. 103312.

[27] Y. Sun, A.F. Pan, Y.Z. Ma, J. Chang, K.M. Li, and S.T. Hu, Activation mechanism of diasporic bauxite calcined with sodium carbonate, *Miner. Eng.*, 187(2022), art. No. 107782.

[28] Y. Xue, X.M. Liu, C.B. Xu, and Y.H. Han, Hydrometallurgical detoxification and recycling of electric arc furnace dust, *Int. J. Miner. Metall. Mater.*, 30(2023), No. 11, p. 2076.

[29] L. Cancellara, T. Markurt, T. Schulz, *et al*., Role of oxygen diffusion in the dislocation reduction of epitaxial AlN on sapphire during high-temperature annealing, *J. Appl. Phys.*, 130(2021), No. 20, art. No. 203101.

[30] H. Lv, M.Z. Xie, L.T. Shi, *et al*., A novel green process for the synthesis of high-whiteness and ultrafine aluminum hydroxide powder from secondary aluminum dross, *Ceram. Int.*, 48(2022),

No. 1, p. 953.
[31] A. Mary Ealias and M.P. Saravanakumar, Facile synthesis and characterisation of AlNs using Protein Rich Solution extracted from sewage sludge and its application for ultrasonic assisted dye adsorption: Isotherms, kinetics, mechanism and RSM design, *J. Environ. Manage.*, 206(2018), p. 215.
[32] J.L. Huang, N.W. Zhu, X. Li, Y.H. Xi, W.Q. Shen, and P.X. Wu, Triggered heavy metals and chlorine simultaneous removal from hazardous waste incineration fly ash, *Process Saf. Environ. Prot.*, 175(2023), p. 796.
[33] W.Q. Shen, N.W. Zhu, Y.H. Xi, *et al*., Effects of medical waste incineration fly ash on the promotion of heavy metal chlorination volatilization from incineration residues, *J. Hazard. Mater.*, 425(2022), art. No. 128037.
[34] Y.H. Xi, N.W. Zhu, J.L. Huang, X. Li, W.Q. Shen, and P.X. Wu, Na_2O induced stable heavy metal silicates phase transformation and glass network depolymerization, *J. Cleaner Prod.*, 380(2022), art. No. 135009.
[35] M.Z. Xie, H. Lv, F.Q. Liu, and H.L. Zhao, Study on phase transformation and reaction behavior of alumina extraction process by calcification of aluminum dross, *J. Mater. Res. Technol.*, 25(2023), p. 6000.
[36] S.W. Li, J. Pan, D.Q. Zhu, *et al*., A new route for separation and recovery of Fe, Al and Ti from red mud, *Resour. Conserv. Recycl.*, 168(2021), art. No. 105314.
[37] J.J. Zhang, B. Liu, H.L. Shen, *et al*., Theoretical and experimental on the thermodynamic, kinetic and phase evolution characteristics of secondary aluminum ash, *J. Mater. Res. Technol.*, 19(2022), p. 3857.
[38] H.J. Ni, C.Y. Lu, Y. Zhang, *et al*., Effects of sodium carbonate and calcium oxide on roasting denitrification of recycled aluminum dross with high nitrogen content, *Coatings*, 12(2022), No. 7, art. No. 922.
[39] E. David and J. Kopac, Aluminum recovery as a product with high added value using aluminum hazardous waste, *J. Hazard. Mater.*, 261(2013), p. 316.
[40] M.A. Khairul, J. Zanganeh, and B. Moghtaderi, The composition, recycling and utilisation of Bayer red mud, *Resour. Conserv. Recycl.*, 141(2019), p. 483.
[41] M.K. Murukutti and H. Jena, Synthesis of nano-crystalline zeolite-A and zeolite-X from Indian coal fly ash, its characterization and performance evaluation for the removal of Cs^+ and Sr^{2+} from simulated nuclear waste, *J. Hazard. Mater.*, 423(2022), art. No. 127085.
[42] X.H. Fan, G. Wong, M. Gan, X.L. Chen, Z.Y. Yu, and Z.Y. Ji, Establishment of refined sintering flue gas recirculation patterns for gas pollutant reduction and waste heat recycling, *J. Cleaner Prod.*, 235(2019), p. 1549.
[43] W.J. Yang, J.H. Zhou, M.S. Liu, Z.J. Zhou, J.Z. Liu, and K.F. Cen, Combustion process and nitrogen oxides emission of Shenmu coal added with sodium acetate, *Energy Fuels*, 21(2007), No. 5, p. 2548.